

1 **Title:** Black carbon concentrations and modeled smoke deposition fluxes to the bare ice dark  
2 zone of the Greenland Ice Sheet

3 **Authors:** Alia L. Khan<sup>1</sup>, Peng Xian<sup>2</sup>, Joshua Schwarz<sup>3</sup>

4 <sup>1</sup>Department of Environmental Sciences, Western Washington University

5 <sup>2</sup>Aerosol and Radiation Section of the Marine Meteorology Division, Naval Research  
6 Laboratory, Monterey, California, USA

7  
8 <sup>3</sup>Chemical Sciences Division, NOAA Earth System Research Laboratory (ESRL), Boulder, CO,  
9 United States

10  
11 **Correspondence to:** Alia L. Khan ([alia.khan@wwu.edu](mailto:alia.khan@wwu.edu))

12  
13 **Abstract:**

14 Ice-albedo feedbacks in the ablation region of the Greenland Ice Sheet (GrIS) are difficult to  
15 constrain and model due in part to our limited understanding of the seasonal evolution of the  
16 bare-ice region. To help fill observational gaps, 13 surface samples were collected on the GrIS  
17 across the 2014 summer melt season from patches of snow that were visibly light, medium, and  
18 dark colored. These samples were analyzed for their refractory black carbon (rBC)  
19 concentrations and size distributions with a Single Particle Soot Photometer coupled to a  
20 characterized nebulizer. We present a size distribution of rBC in fresh snow on the GrIS, as well  
21 as from surface hoar in the bare ice dark zone of the GrIS. The size distributions from the  
22 surface hoar samples appear unimodal, and were overall smaller than the fresh snow sample,  
23 with a peak around 0.3  $\mu\text{m}$ . The fresh snow sample contained very large rBC particles that had a  
24 pronounced bimodality in peak size distributions, with peaks around 0.2  $\mu\text{m}$  and 2  $\mu\text{m}$ . rBC  
25 concentrations ranged from a minimum of 3  $\mu\text{g-rBC/L-H}_2\text{O}$  in light-colored patches at the  
26 beginning and end of the melt season, to a maximum of 32  $\mu\text{g-rBC/L-H}_2\text{O}$  in a dark patch in  
27 early August. On average, rBC concentrations were higher ( $20 \mu\text{g-rBC/L-H}_2\text{O} \pm 10 \mu\text{g-rBC/L-}$

28 H<sub>2</sub>O) in patches that were visibly dark compared to medium patches (7 μg-rBC/L-H<sub>2</sub>O ± 2 μg-  
29 rBC/L-H<sub>2</sub>O) and light patches (4 μg-rBC/L-H<sub>2</sub>O ± 1 μg-rBC/L-H<sub>2</sub>O), suggesting BC aggregation  
30 contributed to snow aging on the GrIS, and vice versa. Additionally, concentrations peaked in  
31 light and dark patches in early August, which is likely due to smoke transport from wildfires in  
32 Northern Canada and Alaska as supported by the Navy Aerosol Analysis and Prediction System  
33 (NAAPS) reanalysis model. According to model output, 26 mg/m<sup>3</sup> of biomass burning derived  
34 smoke was deposited between April 1<sup>st</sup> and August 30<sup>th</sup>, of which 85% came from wet  
35 deposition and 67% was deposited during our sample collection timeframe. The increase in rBC  
36 concentration and size distributions immediately after modelled smoke deposition fluxes suggest  
37 biomass burning smoke is a source of BC to the dark zone of the GRIS. Thus, [the](#) role of BC in  
38 the seasonal evolution of the ice-albedo feedback should continue to be investigated in the bare-  
39 ice zone of the GrIS.

40

#### 41 **1. Introduction**

42 The bare ice dark zone of the southwest Greenland Ice Sheet (GrIS) is characterized by low  
43 albedo due in part to the presence of light absorbing impurities (LAIs), that create a positive ice-  
44 albedo feedback through increased surface melting, ice grain growth, and darkening (Tedesco et  
45 al., 2016). LAIs in this region are a mixture of cryoconite, ice algae (Stibal et al., 2017; Ryan et  
46 al., 2018), dust (Wientjes et al., 2011), and black carbon (BC) such as from Northern  
47 Hemisphere fires (Khan et al., 2017), yet the relative contribution of each light absorbing particle  
48 is still uncertain. The radiative forcing of these LAIs, along with warming summer surface  
49 temperatures (Hanna et al., 2008), leads to large volumes of supra-glacial melt (Greuell, 2000).

50 Furthermore, retreat of the snowline is amplifying surface melt of the GrIS due to increased bare  
51 ice exposure (Ryan et al., 2019) and the LAI-ice albedo feedbacks described above.

52 BC in and on snow and ice is known to warm the Arctic and contribute to snow and ice  
53 melting, however the magnitude of its influence is still highly uncertain e.g., (Flanner et al.,  
54 2007; Bond et al., 2013). BC concentration in air is typically operationally defined depending on  
55 the analytical technique used (Petzold et al., 2013). Many in-situ measurements of BC  
56 concentration in snow in the Arctic have been reported by the Integrating Plate and Integrating  
57 Sandwich (IS) technique, which provides analysis of light absorption of particulate impurities  
58 through spectrophotometric analysis of filter loaded with particulates collected from melted  
59 samples (e.g., Clarke and Noone, 1985; Doherty et al., 2010; Doherty et al., 2013). Doherty et al.

60 (2010) reported a median concentration of 3 ng/g in surface snow, with higher concentration  
61 layers up to ~20ng/g in snow profiles at Dye 2. Snow samples from snowpits in the northwest  
62 sector of the GrIS were also collected in 2013 and 2014 from two traverses and analyzed for

63 elemental/organic carbon (EC/OC). The mean concentration of the samples collected was 2.6  
64 ng/g and the mean peak was 15 ng/g. Based on these results, it was determined that EC/OC do  
65 not influence the snow albedo in the NW sector of the GrIS dry zone, (Polashenski et al., 2015a).

66 Observations of refractory black carbon (rBC) analyzed by the Single Particle Soot Photometer  
67 (SP2) have been published from snow profiles and ice cores in the accumulation region closer to  
68 the Summit research station (McConnell et al., 2007a; Keegan et al., 2014b; Lim et al., 2014).  
69 McConnell et al. (2007) presented BC concentrations from a 215-year ice-core record collected  
70 at D4 in West Central Greenland with average concentrations of 1.7ng/g in pre-industrial times,  
71 2.3ng/g over the period 1950-2002, and around 5 ng/g in the peak period of the early 1900s. The  
72 maximum monthly concentration observed was 58.8 ng/g in 1854, however, monthly

Deleted: s

Deleted: and

Deleted: t

Deleted: is region with

Deleted: a mean of 2.6 ng/g and a mean peak of 15 ng/g

78 concentrations only exceeded 5 ng/g ~2-3 times each decade after 1950. Polashenski et al.,  
79 (2015) provides a comprehensive review of previous BC concentrations in their supplemental  
80 info, showing that the BC average ranges between 1.5 and 3 ng/g over an annual cycle, with peak  
81 deposition occurring during summer episodic events, with concentrations of 5 - 10+ ng/g only  
82 occurring a few times at a given site per decade. [Similarly, rBC concentrations from the](#)  
83 [percolation zone of the GrIS have been shown to be relatively low, less than 1.5 ng/g \(Lewis et](#)  
84 [al., 2021\).](#)

85 rBC measured by SP2 has been shown to provide more reliable measurements of  
86 concentration than the IS or EC/OC (from liquid and air samples, respectively) techniques  
87 because it is largely free from the interference of materials other than rBC (Kondo et al., 2011;  
88 Schwarz et al., 2012) such as pyrolyzed organic carbon artifacts (Lim et al., 2014). It also  
89 provides a lower detection limit and increased sensitivity at low concentrations (Lim et al. 2014).  
90 The SP2 coupled with a nebulizer also provides a measurement of rBC particle size distribution  
91 from liquid samples.

92 rBC particle size has been observed in some snow samples to be larger than expected  
93 from atmospheric measurements, reflecting to some degree size-dependent removal processes  
94 from the atmosphere (Schwarz et al., 2013). The rBC size distribution in snow, which at this  
95 point is constrained by direct observations not supported by detailed modeling, is a significant  
96 source of uncertainty for calculating the overall radiative forcing of BC-in-snow on the Arctic  
97 climate, as well as the global climate (e.g., Bond et al., 2013). Very few rBC size distributions in  
98 snow have been reported globally, with most measurements coming from the Arctic (Lim et al.,  
99 2014; Khan et al., 2017; Mori et al., 2019).

100 Although, observations of BC in snow have been previously observed in the percolation zone  
101 (Dye 2) and accumulation zone (Summit Station) by the IS technique (Doherty et al., 2010a, 2013)  
102 and rBC-SP2 at Summit Station (McConnell et al., 2007b; Keegan et al., 2014a; Lim et al., 2014),  
103 to the authors' knowledge, no reports of rBC concentrations with size distributions in snow and  
104 surface hoar have been reported from the GrIS, providing new insight, particularly into the  
105 dynamic bare-ice region.

106 Here we present rBC concentrations with size distributions from the bare ice region of the  
107 GrIS before and after influence by a major wildfire event, along with NAAPS modelled wet and  
108 dry deposition. Our findings suggests that rBC surface hoar concentrations in the bare ice zone  
109 reflect atmospheric conditions momentarily, before being reset, possibly by supra-glacial melt.  
110 Additionally, NAAPS model output suggest most of the biomass burning derived smoke  
111 deposition comes in the form of wet removal (i.e., removal by precipitation). These rBC  
112 concentrations and size distributions provide insight into the seasonal evolution of impurities,  
113 which are needed to constrain ice-albedo feedbacks in the bare-ice zone of the GrIS.

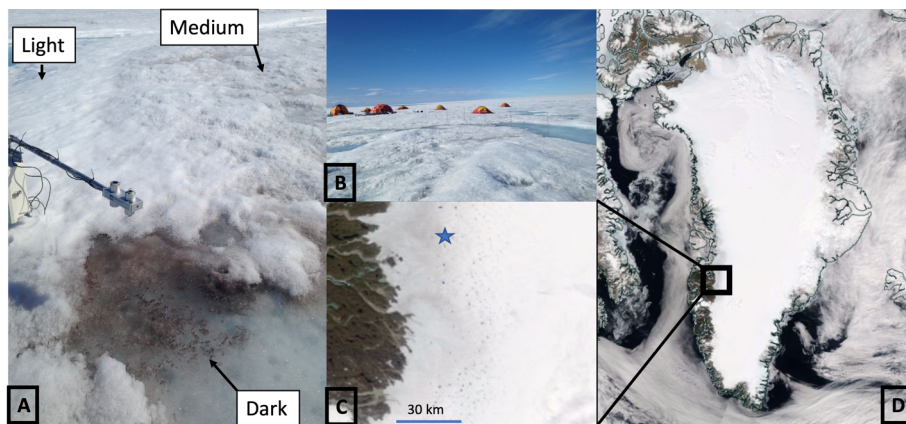
114

## 115 **2. Methods**

### 116 *2.1 Site Description and Snow Sampling*

117 The field site was in the southwestern region of the GrIS near the S6 automated weather station  
118 at 67 04.779°N, 49 24.077°W, and 1011 m above sea level. More information on the study site  
119 can be found in Stibal et al. (2017). A fresh snow surface sample (2 – 3 cm), was collected just  
120 after a snow event on 2014-06-27. Three surface hoar samples (2 – 3 cm), were collected in [150](#)  
121 [mL](#) pre-cleaned and combusted amber glass bottles four times between 2014-06-28 and 2014-08-  
122 11 across the 2014 summer melt season from visually identified light, medium, and dark patches

123 of surface hoar, for a total of 13 samples, including the fresh snow. While all sample sites could  
 124 include a mixture of ice algae, dust, black carbon (i.e., cryoconite), the dark patches especially  
 125 could represent refrozen melt that is enhanced in LAIs, including rBC. A mixture of light,  
 126 medium and dark 1 – 3 m<sup>2</sup> patches were sampled within the ~.5 km<sup>2</sup> study area to characterize  
 127 the breadth of surface types and heterogenous distribution of impurities. Samples were stored  
 128 frozen in a ‘field cooler’ dug into the ice and then transported frozen on ice to Kangerlussuaq,  
 129 and shipped on dry ice to the Denver Airport, and then transported immediately to a freezer at  
 130 the Institute of Arctic and Alpine Research (INSTAAR) at the University of Colorado – Boulder.



A and B are images collected by Dr. Alia Khan. C and D are MODIS satellite images acquired from the NASA Worldview application.

131  
 132 **Figure 1:** A) Example light, medium and dark patches of ice. B) The Dark Snow Field Camp. C)  
 133 The southwest GrIS dark zone with the field sampling location indicated by a blue star and D)  
 134 the GrIS from MODIS on July 2<sup>nd</sup>, 2014.

135  
 136 *2.2 Processing for Refractory Black Carbon*

137 The samples were transported frozen from INSTAAR to the Earth System Research Laboratory  
 138 at the National Oceanic and Atmospheric Administration where they were analyzed for rBC

**Deleted:** A and B are photos collected by Alia Khan. C and D are MODIS satellite images acquired from the NASA Worldview application (<https://worldview.earthdata.nasa.gov/>), part of the NASA Earth Observing System Data and Information System (EOSDIS)....

145 mass mixing ratios (MMRs) by SP2 coupled to a nebulizer per the methods described in Katich  
146 et al. (2017) and Khan et al. (2018). Briefly, the samples were melted for the first time just prior  
147 to analysis with the SP2 and aerosolized with a carefully calibrated concentric pneumatic  
148 nebulizer based on a customized U5000 AT+ nebulizer (Teledyne Cetac, Inc.) which the  
149 ultrasonic piezo was replaced with a concentric pneumatic nebulizer. The SP2 was calibrated  
150 with fullerene soot (Lot# F12S011, Alfa Aesar Inc., Wood Hill, MA) with the community  
151 calibration approach (Baumgardner et al., 2012) over masses of 1 – 20 fg. Using a power law  
152 calibration dependence following Schwarz et al., [2012], the resulting linear calibration of SP2  
153 signal to rBC mass applied to mass of 80 fg was extended further to 4000 fg. The SP2 was  
154 operated with a widely staggered gain for two incandescent channels, allowing sizing of rBC  
155 mass in the range ~1 – 4000 fg.

156 Melted snow samples were interspersed with deionized water blanks to confirm a low  
157 background, especially relative to the MMRs, indicating no appreciable contamination to  
158 concentrations and size distributions. Little size-dependence in nebulization efficiency was  
159 confirmed with concentration standards of polystyrene latex spheres (PSLs) over 220 – 1500 nm  
160 diameter, which is consistent with recent results from concentric pneumatic nebulizers (Wendl et  
161 al., 2014, Katich et al., 2017). Therefore, size dependent corrections were not necessary. During  
162 data acquisition with the SP2, its lower mass-detection limit was 1.2 fg, which corresponds to  
163 about a 110 nm volume equivalent diameter (VED) size detection limit, assuming 1.8g/cc void  
164 free density. A 510 nm diameter PSL concentration standard was sampled between melted snow  
165 analyses to track possible changes in nebulization efficiency during each day of sampling. This  
166 revealed effectively constant efficiency varying with a standard deviation less than 5%. A  
167 gravimetric mass concentration standard (Schwarz et al., 2012) was also used to evaluate

168 nebulization efficiency. The results of the PSL and gravimetric calibrations of nebulizer  
169 efficiency were consistent within uncertainties of 20% and were averaged to provide a best-  
170 estimate nebulization efficiency that was then used to produce the BC MMR values as in  
171 Schwarz et al. (2012).

172

### 173 *2.3 Global Aerosol Modeling*

174 The Navy Aerosol Analysis Prediction System (NAAPS) model is a global aerosol transport  
175 model which provides 6-hrly biomass burning smoke, anthropogenic and biogenic fine aerosols,  
176 dust, and sea salt aerosol forecasts and analyses below 100 hPa at 1/3° latitude/longitude spatial  
177 resolution and contains 42 vertical atmospheric levels. The NAAPS reanalysis (NAAPS-RA) is  
178 available 2003-current with a coarser spatial resolution (1° latitude/longitude horizontal and 25  
179 vertical levels) (Lynch et al., 2016). Total column aerosol optical thickness (AOT) is constrained  
180 through assimilation of quality-controlled satellite AOT retrievals from the Moderate [Resolution](#)  
181 Imaging Spectroradiometer (MODIS) and Multi-angle Imaging SpectroRadiometer (MISR).  
182 Near-real time satellite based thermal anomaly data enables detection of wildfires and  
183 construction of biomass burning smoke emissions (Reid et. al., 2009). Orbital corrections for  
184 MODIS-based fire detections and regional factors were applied on emissions so that the  
185 reanalysis AOT verifies well with ground-based measurements (Lynch et al., 2016). The  
186 NAAPS-RA has been applied to a broad range of science applications, and specifically the life  
187 cycle, climatology, radiative forcing, aerosol-atmosphere-ice-ocean interactions of biomass  
188 burning smoke aerosols (e.g., Reid et al., 2012; Xian et al., 2013; Markowicz et al., 2021; Ross et  
189 al., 2018; Khan et al., 2019; Carson-Marquis et al., 2021), as well as previously to corroborate  
190 wildfire smoke transport to the GrIS (Khan et al., 2017), Arctic Canada (Ranjbar et al., 2019),



191 Svalbard (Markowicz et al., 2016; 2017), the pan-Arctic region (Xian et al., 2022a, b), the  
192 Nepalese Himalayas (Khan et al., 2020), and the Antarctic (Khan et al., 2018; Khan et al., 2019).  
193 Speciated AOT, surface aerosol concentration and deposition flux are used in this study. Here the  
194 deposition is calculated as 24-hour flux to the surface of the ice sheet in mg/m<sup>2</sup>/day. ~~Estimating  
195 atmospheric properties related to biomass burning is highly complex and is influenced by wide  
196 variety of factors such as the type of fuel, combustion temperature, and atmospheric  
197 conditions. Also, the chemical, optical and physical properties of biomass burning aerosols can  
198 change during atmospheric transport and dispersion. The mass ratio of rBC to total mass in  
199 biomass burning smoke particles is estimated to be 5–10% black carbon in the NAAPS-RA  
200 model based on field studies (see a summary in Reid et al., 2005) and here we chose 7% as a  
201 median value.~~

**Deleted:** The mass ratio of rBC to total mass in biomass burning smoke particles is assumed to be 7%, which is an approximate median value from literatures (i.e., Reid et al., 2005)

**Formatted:** Font: 12 pt

**Formatted:** Font: 12 pt

**Formatted:** Font: 12 pt

### 202 3. Results and Discussion

#### 203 3.1 rBC Concentrations

204 rBC concentrations in the surface hoar ranged from a minimum of 3 µg-rBC/L-H<sub>2</sub>O in light  
205 patches at the beginning and end of the melt season, to a peak of 32 µg-rBC/L-H<sub>2</sub>O in a dark  
206 patch in early August (Table 1). rBC concentrations were higher in patches that were visibly  
207 darker (20 µg-rBC/L-H<sub>2</sub>O) compared to medium patches (7 µg-rBC/L-H<sub>2</sub>O) and light patches (4  
208 µg-rBC/L-H<sub>2</sub>O), suggesting BC aggregates with dust and biological material on the GrIS. Light  
209 and dark patch concentrations peaked in early August. Our minimum concentrations are in the  
210 range of rBC concentrations found elsewhere on the GrIS, but our peaks are higher than  
211 previously reported concentrations from snow on the GrIS (Doherty et al., 2010a; Polashenski et  
212 al., 2015; Lewis et al., 2021). Our maximum concentrations are higher than the highest  
213 concentrations observed in vertical snow with the IS (Doherty et al., 2010b) and EC/OC

218 technique (Polashenski et al., 2015), but less than the highest monthly average concentration of  
 219 year of 1854 reported in an ice core by McConnell et al. (2007). The concentration of rBC in the  
 220 fresh snow (3  $\mu\text{g-rBC/L-H}_2\text{O}$ ) sample was roughly the same as the light surface hoar patches on  
 221 2014-06-28 and 2014-08-11.

222

223 **Table 1:** NAAPs Smoke Dry, Wet, and Total Deposition ( $\text{mg/m}^2/\text{day}$ ) from April 1<sup>st</sup> prior to  
 224 sample collection. Average rBC concentrations from visually light, medium, and dark patches of  
 225 surface hoar. All samples were collected at 67.07979701 degrees N and -49.40116603 degrees W  
 226 at 1005 meters above sea level in the dark zone ablation region of the SW Greenland Ice Sheet.

227 ^The fresh snow sample is a single sample.

Date	NAAPS	NAAPS <del>s</del>	NAAPS <del>s</del>	Average	Snow type (visual color)	rBC
	Smoke Dry Deposition ( $\text{mg/m}^3/\text{day}$ )	Smoke Wet Deposition ( $\text{mg/m}^3/\text{day}$ )	Smoke Total Deposition ( $\text{mg/m}^2/\text{day}$ )	rBC $\mu\text{g-rBC/L-H}_2\text{O}$		rBC $\mu\text{g-rBC/L-H}_2\text{O}$
6/27/14	0.58	1.98	2.56	3.05 <sup>^</sup>	Fresh	3.05
6/28/14	0.60	6.92	7.51	8.37	Light	2.87
					Medium	9.61
					Dark	12.62
7/21/14	0.75	6.93	7.69	11.45	Light	4.21
					Medium	6.42
					Dark	23.71
8/2/14	1.51	9.44	10.95	14.15	Light	5.27
					Medium	4.71
					Dark	32.47
8/11/14	1.94	12.14	14.08	8.12	Light	2.96

Deleted: s

Deleted: s

Medium	8.75
Dark	12.64

230

### 231 3.2 rBC Size Distributions

232 We found very large rBC are present (Figure 2A, B and C), especially in the fresh snow sample.

Deleted: and

233 The large size distribution in fresh snow follows previous findings in the rocky mountains that

Deleted: s

234 rBC size distributions can be larger in surface snow than expected in aerosol in the atmosphere

235 (Schwarz et al., 2013). Furthermore, the fresh event is associated with a more pronounced

236 bimodality at  $\sim 0.2 \mu\text{m}$  and  $2 \mu\text{m}$  (Figure 2A), whereas the rBC in surface hoar samples appears

237 more unimodal (Figure 2B and 2C). The average surface hoar rBC sizes, which have not been

238 previously reported in the literature, are smaller than the one fresh snow sample with a peak

239 around  $0.3 \mu\text{m}$ . This is still larger than typical modal sizes for rBC observed in the atmosphere

240 (in the range  $\sim 0.11 - 0.2 \mu\text{m}$  typically). Furthermore, no apparent patterns emerge in the size

241 distributions across the light, medium and dark patches over the duration of the season.

242 However, the surface hoar rBC size distributions likely evolve, just as the seasonal snow cover

243 evolves into bare ice and surface hoar, but we are unable to assess from this relatively small data

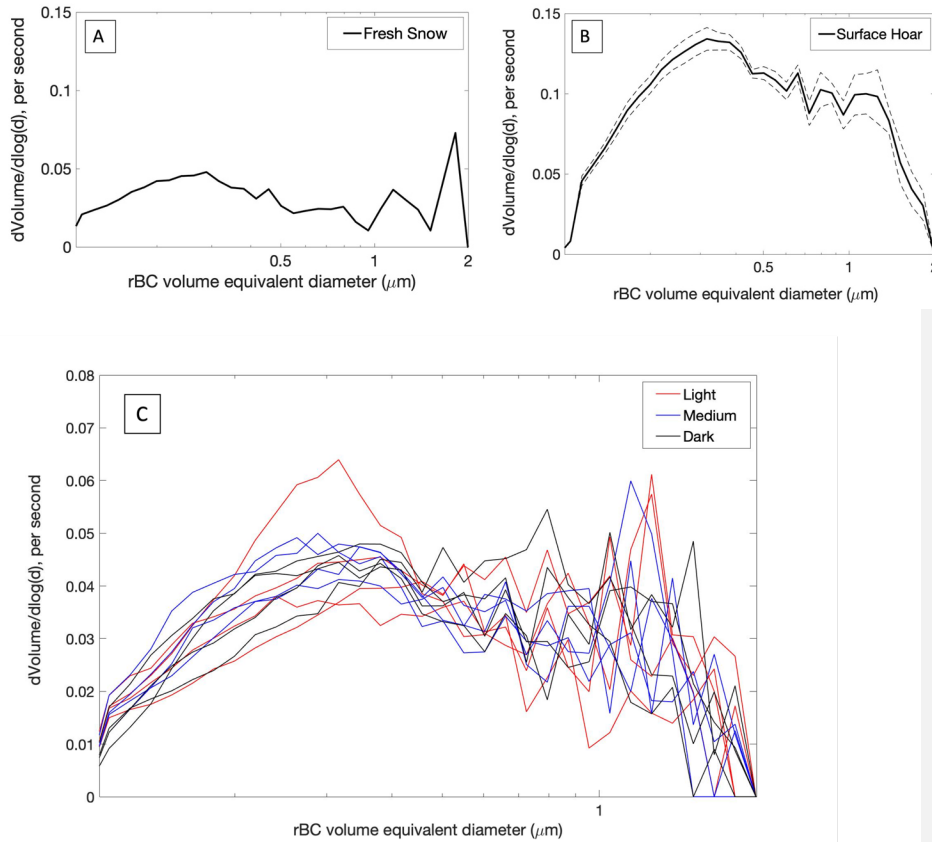
244 set. This conjecture is supported by observations that repeated freeze/thaw cycles tend to cause

245 rBC coagulation in liquid (Schwarz et al., 2013). Regardless, these initial results of rBC size

246 distributions from fresh snow and surface hoar in the bare ice region of the GrIS are important

247 for informing ice-albedo models, which are still being developed and refined for bare ice regions

248 of the ice sheet (e.g. Flanner et al., 2007).



251

252

253 **Figure 2:** A) rBC size distribution of fresh snow (n=1), B) all surface hoar samples over the  
 254 duration of the season (n=12) and C) the size distribution of each surface hoar sample  
 255 categorized as light, medium and dark. The dashed lines in Figure 2B represent the max and min  
 256 size distributions and the solid black line is the average.

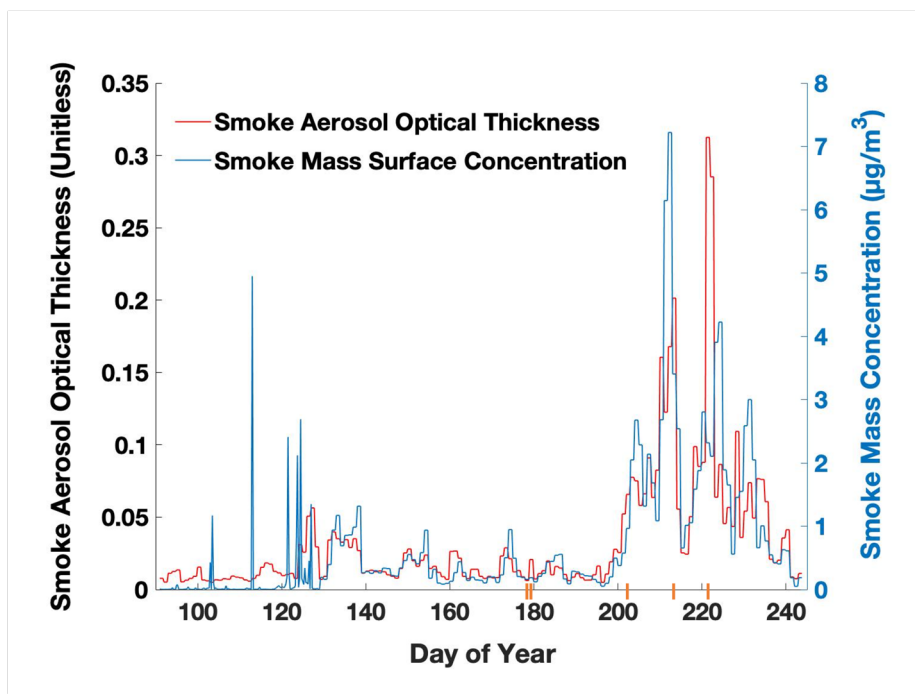
Deleted: and

257

258 3.3 NAAPS Aerosol Model Comparison and Evaluation

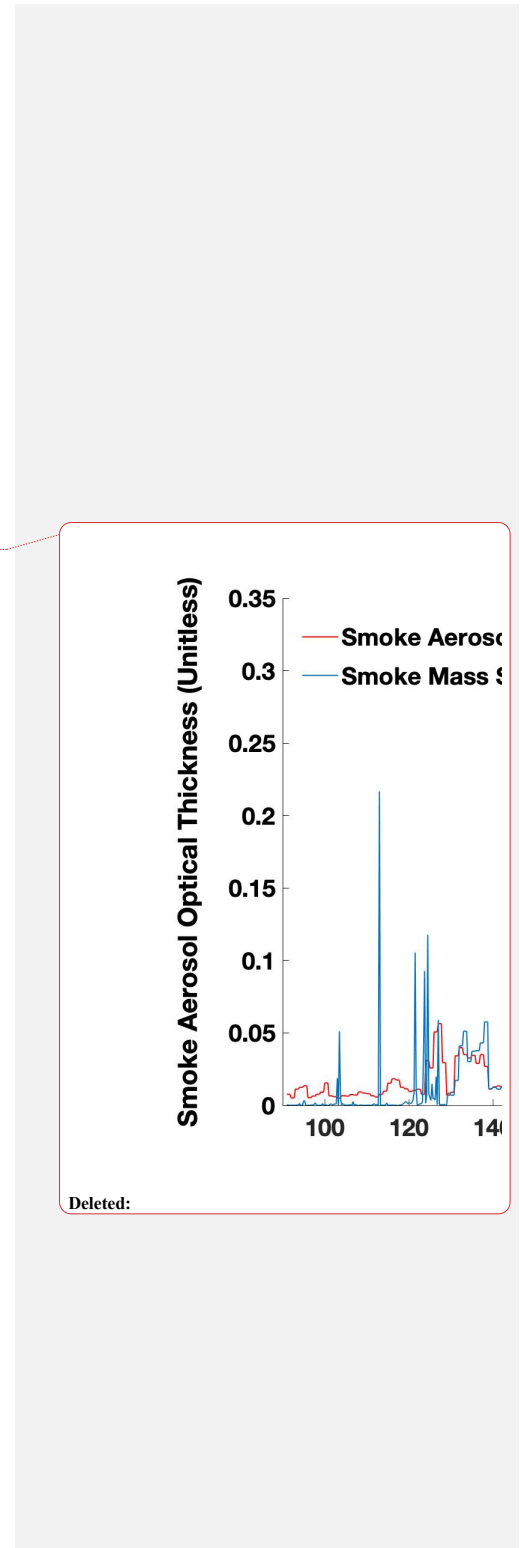
260 The ground observations were then compared to cumulative aggregates of smoke deposition  
261 fluxes modelled with the Navy Aerosol Analysis Prediction System reanalysis model. AOT  
262 derived from MODIS and modeled by NAAPS demonstrates that a large wildfire smoke event  
263 was observed just before the third sample was collected and during the time the fourth sample  
264 was collected (Figure 3). Concomitant AOT and surface concentration predictions from the  
265 NAAPS model confirms our peak concentrations are likely due to Northern Hemisphere wildfire  
266 smoke (Figure 4 A- D).

267

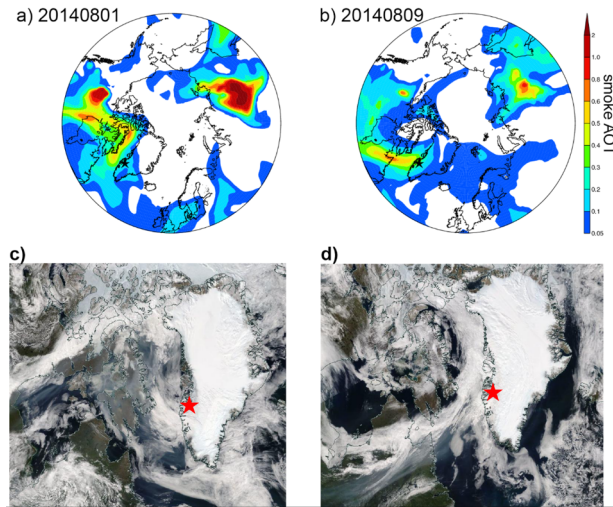


268

269 **Figure 3:** Aerosol optical thickness (AOT) derived from NAAPS reanalysis



271 over the sampling season from smoke and dust. B) Smoke mass concentration ( $\mu\text{g}/\text{m}^3$ ) in the  
272 surface layer of the model (centered around 16m). The five sampling dates are marked in orange.



273  
274 **Figure 4:** Biomass burning smoke transport reaching the GrIS from the west based on NAAPS-  
275 RA daily-mean smoke AOT and MODIS TERRA true color imageries for **A and C** Aug. 1,  
276 2014 and **B and D** Aug. 9, 2014. The sampling location is marked with a black star in the  
277 NAAPS-RA plots (A and B), and red stars in the MODIS imageries (C and D).

278 According to NAAPS model output, the deposition flux of smoke (Table 1 and Fig. 5)  
279 onto the ice surface of the dark zone during our model study period, April 1<sup>st</sup> – August 30<sup>th</sup>, was  
280 25.6 mg/m<sup>2</sup>/day and 85% came from wet deposition. April 1<sup>st</sup> to August 30<sup>th</sup> was chosen based  
281 on the primary Northern Hemisphere wildfire season and smoke transport to the Arctic (Xian et  
282 al., 2022b). 68% of this smoke (17.3 mg/m<sup>2</sup>/day) was deposited during our sample collection  
283 period from June 27<sup>th</sup> to August 11<sup>th</sup>. Prior to the first sample collected on June 27<sup>th</sup>, 10% of the  
284 total smoke flux (2.6 mg/m<sup>2</sup>/day) was deposited from April 1<sup>st</sup> to June 26<sup>th</sup>. After the last sample  
285 was collected on August 11<sup>th</sup>, 5.8 mg/m<sup>2</sup>/day of smoke was deposited between August 12<sup>th</sup> and  
286 30<sup>th</sup>.

Deleted: D

288 We evaluate the NAAPS-RA deposition flux based on the rBC concentration observed in  
289 fresh snow, which was 3  $\mu\text{g-rBC/L-H}_2\text{O}$ . The NAAPS model assumes 7% of smoke is BC. The  
290 snow event that preceded the fresh snow sample collection, had a modeled precipitation rate of  
291 10 mm/day or 10  $\text{L/m}^2$ . The modeled smoke deposition flux is 3000  $\mu\text{g/m}^2/\text{day}$  or 300  $\mu\text{g/L}$  over  
292 24 hours. At 7% BC of total smoke, that leaves us with 21  $\mu\text{g-BC/L-H}_2\text{O}$ . Therefore, the model  
293 appears to be off by roughly a factor of 7 for this one snow sample. Continued work is in  
294 progress to evaluate the model across a larger sample size of rBC ground observations across the  
295 Arctic.

296 Two case studies of interest arise in the modelled total NAAPS smoke flux when  
297 comparing wet and dry deposition. The first one is a large wet deposition flux and the second is a  
298 considerable dry deposition flux. The first wet deposition flux occurred between June 27<sup>th</sup> and  
299 28<sup>th</sup> (day of year 178 and 179), during a snow event (Fig. 5A and B). Here we see the largest  
300 increase in the total deposition flux of smoke over the study period at 5.0  $\text{mg/m}^3/\text{day}$  in just over  
301 24 hours. 99.8% of this comes from wet deposition. When we compare these model findings to  
302 the observational rBC data in the surface hoar and snow, we see the rBC concentration in fresh  
303 snow, 3  $\mu\text{g-rBC/L-H}_2\text{O}$ , is high compared to pristine fresh snow previously found in Svalbard, 1  
304  $\mu\text{g-rBC/L-H}_2\text{O}$  (Khan et al., 2017). The average rBC concentration across the light, medium and  
305 dark patches is also relatively high for a non-human impacted site in the polar regions (Cordero  
306 et al., 2022). A previous study of black carbon in supra-glacial melt from the same GRIS site  
307 previously confirmed the dissolved BC molecular signature was indicative of wildfire smoke that  
308 likely came from Northern Canada and Alaska (Khan et al., 2017). Between July 22<sup>nd</sup> and  
309 August 2<sup>nd</sup>, the model again shows a large proportion of the total deposition flux coming from  
310 wet deposition, 77% of the 3.2  $\text{mg/m}^2/\text{day}$ . Similarly, from August 3<sup>rd</sup> to 11<sup>th</sup>, 86% of the 3.1

Deleted:

Deleted:

Deleted: If we assume the snow water equivalent is 10%, then the rBC-snow concentration (i.e., the concentration of rBC in the fresh wet snow being deposited) would be 2.1  $\mu\text{g-rBC/L-H}_2\text{O}$ .

Deleted: s

Deleted: occurred

319 mg/m<sup>3</sup>/day smoke deposition flux was from wet deposition (Fig. 5A). Again, this follows an  
320 increase in the total precipitation (Fig. 5B).

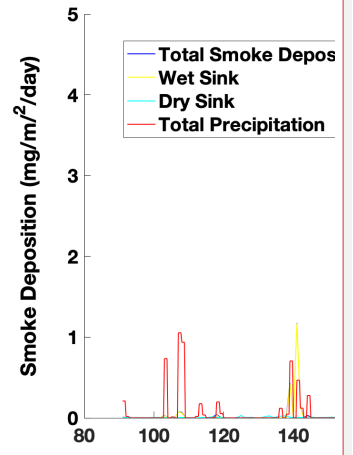
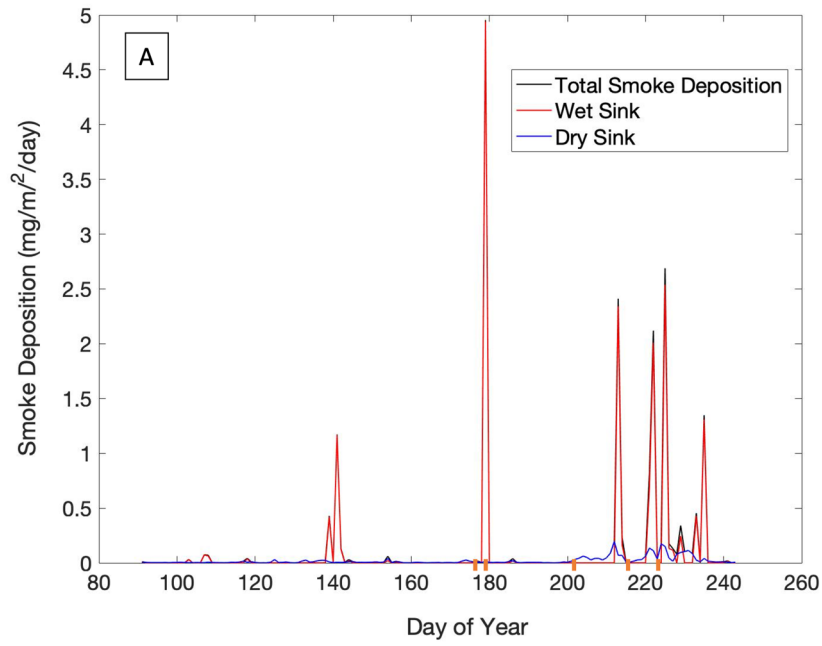
321 However, a dry deposition case arises on July 21<sup>st</sup>, 2014 (DOY 172). Here the NAAPS,  
322 model does not produce a large total smoke deposition flux, but the rBC concentrations are still  
323 relatively high. Since the previous sampling event on June 28<sup>th</sup> (DOY 179), the model produces  
324 0.2 mg/m<sup>3</sup>/day total deposition flux, where only 16% comes from wet deposition. The majority,  
325 84%, is from dry smoke deposition. This finding is also supported by the fact that there was little  
326 precipitation during this time based on the NAAPS modeled meteorology (Fig. 5B), but it is also  
327 important to note that snow aging could also play a role in aggregation of BC particles. The  
328 decrease observed in the surface hoar rBC concentrations in the August 11<sup>th</sup> samples may  
329 suggest there was a process that removed the particles from the surface hoar, such as flushing or  
330 redistribution by supra-glacial melt, or uncontaminated fresh snow deposition which could dilute  
331 the concentrations. Further investigation into this process is warranted.

Deleted: s

Deleted: ,

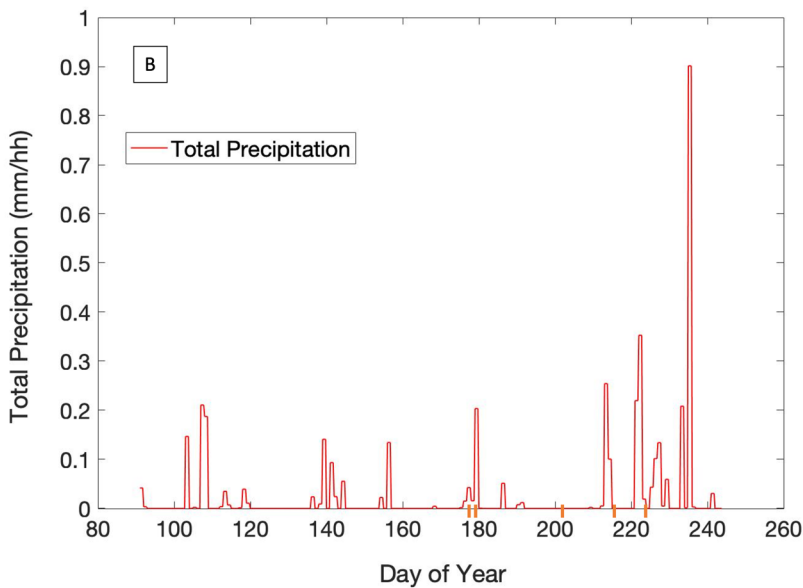
Deleted: s





Deleted:

335



337

338 **Figure 5:** A) Biomass burning derived smoke deposition flux separated as wet and dry  
 339 deposition and B) total precipitation produced by the NAAPS model. The total smoke deposition  
 340 closely follows the wet deposition line. The five sampling dates are marked in orange.

**Deleted:**

**Deleted:** The total deposition flux is separated as wet and dry deposition.

341

342 **4 Conclusion**

343 Here we present (to the author's knowledge) the first rBC size distributions from fresh snow  
 344 and surface hoar in the bare ice region of the GrIS, coupled with their concentrations. An initial  
 345 rBC size distribution in a fresh snow sample from the GrIS shows pronounced bimodality and  
 346 very large particles with the second peak almost 2  $\mu\text{m}$ . These initial rBC size distributions from  
 347 surface hoar in the bare ice dark zone of the Greenland Ice Sheet are smaller than the fresh snow,

351 but still much larger than observations of atmospheric rBC. There appears to be a shift in the  
352 modal peak of rBC particle size in light patches over the duration of the season from  $\sim 0.3 \mu\text{m}$  to  
353  $\sim 1.4 \mu\text{m}$ , further suggesting aggregation of particles in the bare-ice region. NAAPS-AOT<sub>v</sub> and  
354 surface concentration data suggest that rBC surface hoar concentrations in the bare ice zone  
355 reflect atmospheric conditions momentarily, before possibly being reset by supra-glacial melt.

356 Additionally, we demonstrate preliminary verification of BC deposition from the NAAPS<sub>s</sub>  
357 RA with *in-situ* observations. rBC measurements in dark patches from late June to early August  
358 2014 reveal an increase just after the smoke event. These elevated concentrations are closer to  
359 previously reported values in vertical snow and ice-core layers (e.g., Doherty et al., 2010 and  
360 Polashenski et al., 2013). The overall higher concentrations of rBC in visibly darker patches,  
361 where higher concentrations of ice algae were observed (Stibal et al., 2017), suggest potential bio  
362 flocculation with ice algae and mineral dust. However, NAAPS model results also indicate the  
363 increase is likely related to accumulation of episodically deposited wildfire-derived smoke. For  
364 example, the smoke event in early August, which brought smoke from the western Northern  
365 Hemisphere. Based on NAAPS deposition model and corroborated by rBC observations, wet  
366 deposition appears to be the largest source of rBC to the surface. For example, our fresh snow  
367 sample was measured at  $3 \mu\text{g-rBC/L-H}_2\text{O}$ , while the model, off by a factor of 7, produced  $21 \mu\text{g-}$   
368  $\text{rBC/L-H}_2\text{O}$ . These preliminary results suggest global aerosol models may be overestimating BC  
369 deposition; however, further investigation is warranted. These data provide utility in  
370 understanding the seasonal evolution of impurities, which are needed to constrain modeling of  
371 ice-albedo feedbacks in the bare-ice zone of the GRIS.

### 373 Author Contributions

Deleted: D

Deleted: s

Deleted: 0

Deleted: However, NAAPS model results also indicate the increase is likely related to accumulation of deposition of wildfire-derived smoke, especially during episodically, such as the smoke event in early August, which brought smoke from the western Northern Hemisphere.

382 ALK and JS analyzed the rBC samples. PX ran the NAAPS model and provided output data.

Deleted: s

383 ALK wrote the manuscript and PX and JS edited and contributed text. The samples were

384 collected by ALK and the Dark Snow Project.

### 385 Acknowledgements

386 The authors thank the Dark Snow Project for field support and additional sample collection,  
387 specifically, M. Stibal, J. Box and K. Cameron and N. Molotch.

388  
389 **Competing Interests.** There are no conflicts of interest.

### 390 Data Availability

391 **The rBC and NAAPS modeled deposition data are included in Table 1.**

392

### 393 **References**

394  
395 Baumgardner, D., Popovicheva, O., Allan, J., Bernardoni, V., Cao, J., Cavalli, F., et al. (2012).

396 Soot reference materials for instrument calibration and intercomparisons : a workshop

397 summary with recommendations. 1869–1887. doi:10.5194/amt-5-1869-2012.

398 Bond, T. C., Doherty, S. J., Fahey, D. W., Forster, P. M., Berntsen, T., DeAngelo, B. J., et al.

399 (2013). Bounding the role of black carbon in the climate system: A scientific assessment. *J.*

400 *Geophys. Res. Atmos.* 118, 5380–5552. doi:10.1002/jgrd.50171.

401 Cordero, R. R., Sepúlveda, E., Feron, S., Damiani, A., Fernandoy, F., Neshyba, S., ... & Casassa,

402 G. (2022). Black carbon footprint of human presence in Antarctica. *Nature*

403 *communications*, 13(1), 1-11.

404 Doherty, S. J., Grenfell, T. C., Forsström, S., Hegg, D. L., Brandt, R. E., and Warren, S. G.

405 (2013). Observed vertical redistribution of black carbon and other insoluble light-absorbing

406 particles in melting snow. *J. Geophys. Res. Atmos.* 118, 5553–5569.

407 doi:10.1002/jgrd.50235.

408 Doherty, S. J., Warren, S. G., Grenfell, T. C., Clarke, a. D., and Brandt, R. E. (2010a). Light-

409 absorbing impurities in Arctic snow. *Atmos. Chem. Phys.* 10, 11647–11680.

411 doi:10.5194/acp-10-11647-2010.

412 Doherty, S. J., Warren, S. G., Grenfell, T. C., Clarke, A. D., and Brandt, R. E. (2010b). and  
413 Physics Light-absorbing impurities in Arctic snow. 11647–11680. doi:10.5194/acp-10-  
414 11647-2010.

415 Flanner, M. G., Zender, C. S., Randerson, J. T., and Rasch, P. J. (2007). Present-day climate  
416 forcing and response from black carbon in snow. *J. Geophys. Res.* 112, D11202.  
417 doi:10.1029/2006JD008003.

418 Greuell, W. (2000). Melt-water accumulation on the surface of the Greenland ice sheet: Effect on  
419 albedo and mass balance. *Geogr. Ann. Ser. A Phys. Geogr.* 82, 489–498.  
420 doi:10.1111/j.0435-3676.2000.00136.x.

421 Hanna, E., Huybrechts, P., Steffen, K., Cappelen, J., Huff, R., Shuman, C., et al. (2008).  
422 Increased runoff from melt from the Greenland Ice Sheet: A response to global warming. *J.*  
423 *Clim.* 21, 331–341. doi:10.1175/2007JCLI1964.1.

424 Katich, J. M., A. E. Perring, and J. P. Schwarz (2017), Optimized detection of particulates from  
425 liquid samples in the aerosol phase: focus on black carbon, *Aeros. Sci. Technol.*,  
426 doi:10.1080/02786826.2017.1280597

427 Keegan, K. M., Albert, M. R., McConnell, J. R., and Baker, I. (2014a). Climate change and forest  
428 fires synergistically drive widespread melt events of the Greenland Ice Sheet. 1–4.  
429 doi:10.1073/pnas.1405397111.

430 Keegan, K. M., Albert, M. R., McConnell, J. R., and Baker, I. (2014b). Climate change and  
431 forest fires synergistically drive widespread melt events of the Greenland Ice Sheet. *Proc.*  
432 *Natl. Acad. Sci. U. S. A.* 111. doi:10.1073/pnas.1405397111.

433 Khan, A. L., McMeeking, G. R., Schwarz, J. P., Xian, P., Welch, K. A., Berry Lyons, W., &

434 McKnight, D. M. (2018). Near-surface refractory black carbon observations in the  
 435 atmosphere and snow in the McMurdo dry valleys, Antarctica, and potential impacts of  
 436 Foehn winds. *Journal of Geophysical Research: Atmospheres*, 123(5), 2877-2887.

437 Khan, A. L., H. Dierssen, J. P. Schwarz, C. Schmitt, A. Chlus, M. Hermanson, T. H. Painter,  
 438 and D. M. M. (2017). [“Impacts of coal dust on the spectral reflectance of Arctic surface  
 439 snow in Svalbard, Norway”](#). *Journal of Geophysical Research: Atmospheres*, 1–12.  
 440 doi:10.1002/2016JD025757.

441 Khan, A.L., Wagner, S., Jaffé, R., Xian P. , Williams M., and Armstrong, R., and McKnight, D.  
 442 (2017). [“Dissolved black carbon in the global cryosphere: Concentrations and chemical  
 443 signatures”](#), *Geophysical Research Letters*, 1–9. doi:10.1002/2017GL073485.

444 [Lewis, G., Osterberg, E., Hawley, R., Marshall, H. P., Meehan, T., Graeter, K., et al. \(2021\).  
 445 \[Atmospheric blocking drives recent albedo change across the western Greenland ice sheet  
 446 percolation zone. Geophysical Research Letters\]\(#\), 48, e2021GL092814.  
 447 <https://doi.org/10.1029/2021GL092814>](#).

448 Lim, S., Faïn, X., Zanatta, M., Cozic, J., Jaffrezo, J.-L., Ginot, P., et al. (2014). Refractory black  
 449 carbon mass concentrations in snow and ice: method evaluation and inter-comparison with  
 450 elemental carbon measurement. *Atmos. Meas. Tech.* 7, 3549–3589. doi:10.5194/amtd-7-  
 451 3549-2014.

452 [Lynch, P., Reid, J. S., Westphal, D. L., Zhang, J., Hogan, T. F., Hyer, E. J., Curtis, C. A., Hegg,  
 453 D. A., Shi, Y., Campbell, J. R., Rubin, J. I., Sessions, W. R., Turk, F. J., and Walker, A. L.:](#)  
 454 [An 11-year global gridded aerosol optical thickness reanalysis \(v1.0\) for atmospheric and  
 455 climate sciences, Geosci. Model Dev.](#), 9, 1489–1522, [https://doi.org/10.5194/gmd-9-1489-  
 2016](https://doi.org/10.5194/gmd-9-1489-<br/>
  456 2016), 2016.

457 Markowicz, K. M., et al. (2016), Impact of North American intense fires on aerosol optical

Deleted: Journal of Geophysical Research : Atmospheres.

Deleted: J. Geophys. Res. Atmos.

Deleted: Geophysical Research Letters. *Geophys. Res. Lett.*

Formatted: Font: Italic

Formatted: Font: (Default) Times New Roman, 12 pt

Formatted: Font: (Default) Times New Roman, 12 pt

Formatted: Normal (Web), Indent: First line: 0", Line spacing: single, Widow/Orphan control, Adjust space between Latin and Asian text, Adjust space between Asian text and numbers

Formatted: Font color: Custom Color(RGB(70,70,70)), Check spelling and grammar

Formatted: Font: (Default) Times New Roman, 12 pt

462 properties measured over the European Arctic in July 2015, *J. Geophys. Res. Atmos.*, 121,  
463 14,487–14,512, doi:10.1002/2016JD025310.

464 Markowicz, K.M., Lisok, J., Xian, P., Simulation of long-term direct aerosol radiative forcing  
465 over the arctic within the framework of the iAREA project, *Atmospheric Environment*  
466 (2021), doi: <https://doi.org/10.1016/j.atmosenv.2020.117882>.

467 McConnell, J. R., Edwards, R., Kok, G. L., Flanner, M. G., Zender, C. S., Saltzman, E. S., et al.  
468 (2007a). 20th-century industrial black carbon emissions altered Arctic climate forcing.  
469 *Science (80-. )*. 317, 1381–4. doi:10.1126/science.1144856.

470 McConnell, J. R., Edwards, R., Kok, G. L., Flanner, M. G., Zender, C. S., Saltzman, E. S., et al.  
471 (2007b). 20th-Century Industrial Black Carbon Emissions Altered Arctic Climate Forcing.  
472 *Science (80-. )*. 317, 1381 LP – 1384. doi:10.1126/science.1144856.

473 Mori, T., Goto-Azuma, K., Kondo, Y., Ogawa-Tsukagawa, Y., Miura, K., Hirabayashi, M., et al.  
474 (2019). Black Carbon and Inorganic Aerosols in Arctic Snowpack. *J. Geophys. Res. Atmos.*,  
475 2019JD030623. doi:10.1029/2019JD030623.

476 Polashenski, C. M., Dibb, J. E., Flanner, M. G., Chen, J. Y., Courville, Z. R., Lai, A. M., et al.  
477 (2015a). Neither dust nor black carbon causing apparent albedo decline in Greenland’s dry  
478 snow zone: Implications for MODIS C5 surface reflectance. 9319–9327.  
479 doi:10.1002/2015GL065912.Received.

480 Polashenski, C. M., Dibb, J. E., Flanner, M. G., Chen, J. Y., Courville, Z. R., Lai, A. M., et al.  
481 (2015b). Neither dust nor black carbon causing apparent albedo decline in Greenland’s dry  
482 snow zone: Implications for MODIS C5 surface reflectance. *Geophys. Res. Lett.* 42.  
483 doi:10.1002/2015GL065912.

484 Ranjbar, K., O’Neill, N. T., Lutsch, E., McCullough, E. M., AboEl-Fetouh, Y., Xian, P., et al.

485 (2019). Extreme smoke event over the high Arctic. *Atmos. Environ.* 218, 117002.  
486 doi:<https://doi.org/10.1016/j.atmosenv.2019.117002>.

487 Reid, J. S., Koppmann, R., Eck, T. F., and Eleuterio, D. P.: A review of biomass burning  
488 emissions part II: intensive physical properties of biomass burning particles, *Atmos. Chem.*  
489 *Phys.*, 5, 799–825, <https://doi.org/10.5194/acp-5-799-2005>, 2005.

490 Ryan, J. C., Hubbard, A., Stibal, M., Irvine-Fynn, T. D., Cook, J., Smith, L. C., et al. (2018).  
491 Dark zone of the Greenland Ice Sheet controlled by distributed biologically-active  
492 impurities. *Nat. Commun.* 9, 1–10. doi:10.1038/s41467-018-03353-2.

493 Ryan, J. C., Smith, L. C., Van As, D., Cooley, S. W., Cooper, M. G., Pitcher, L. H., et al. (2019).  
494 Greenland Ice Sheet surface melt amplified by snowline migration and bare ice exposure.  
495 *Sci. Adv.* 5, 1–11. doi:10.1126/sciadv.aav3738.

496 Schwarz, J. P., Doherty, S. J., Li, F., Ruggiero, S. T., Tanner, C. E., Perring, a. E., et al. (2012).  
497 Assessing recent measurement techniques for quantifying black carbon concentration in  
498 snow. *Atmos. Meas. Tech. Discuss.* 5, 3771–3795. doi:10.5194/amtd-5-3771-2012.

499 Schwarz, J. P., Gao, R. S., Perring, a E., Spackman, J. R., and Fahey, D. W. (2013). Black  
500 carbon aerosol size in snow. *Sci. Rep.* 3, 1356. doi:10.1038/srep01356.

501 Stibal, M., Box, J. E., Cameron, K. A., Langen, P. L., Yallop, M. L., M., H., R., Khan, A.L.,  
502 Molotch, N. P., Christmas, N.A.M., Quaglia, F.C., , Remias, D., Paul, C.J.P., Van den  
503 Broeke, M., Ryan, J., Hubbard, A., Tranter, M., van As, D., and and Ahlström, A. (2017).  
504 Algae Drive Enhanced Darkening of Bare Ice on the Greenland Ice Sheet. *Geophys. Res.*  
505 *Lett.*, 463–471. doi:10.1002/2017GL075958.

506 Stibal, M., Elster, J., Šabacká, M., and Kaštovská, K. (2007). Seasonal and diel changes in  
507 photosynthetic activity of the snow alga *Chlamydomonas nivalis* (Chlorophyceae) from



508 Svalbard determined by pulse amplitude modulation fluorometry. *FEMS Microbiol. Ecol.*  
509 59, 265–273. doi:10.1111/j.1574-6941.2006.00264.x.

510 Tedesco, M., Doherty, S., Fettweis, X., Alexander, P., Jeyaratnam, J., Noble, E., et al. (2016).  
511 The darkening of the Greenland ice sheet: trends, drivers and projections  
512 (1981–2100). *Cryosph. J.* 9, 5595–5645. doi:10.5194/tcd-9-5595-2015.

513 Wendl, I. a., Menking, J. a., Färber, R., Gysel, M., Kaspari, S. D., Laborde, M. J. G., et al.  
514 (2014). Optimized method for black carbon analysis in ice and snow using the Single  
515 Particle Soot Photometer. *Atmos. Meas. Tech.* 7, 3075–3111. doi:10.5194/amtd-7-3075-  
516 2014.

517 Wientjes, I. G. M., Van De Wal, R. S. W., Reichert, G. J., Sluijs, A., and Oerlemans, J. (2011).  
518 Dust from the dark region in the western ablation zone of the Greenland ice sheet.  
519 *Cryosphere* 5, 589–601. doi:10.5194/tc-5-589-2011.

520  
521 Xian, P., Zhang, J., O'Neill, N. T., Toth, T. D., Sorenson, B., Colarco, P. R., Kipling, Z., Hyer, E.  
522 J., Campbell, J. R., Reid, J. S., and Ranjbar, K.: Arctic spring and summertime aerosol  
523 optical depth baseline from long-term observations and model reanalyses – Part 1:  
524 Climatology and trend, *Atmos. Chem. Phys.*, 22, 9915–9947, [https://doi.org/10.5194/acp-](https://doi.org/10.5194/acp-22-9915-2022)  
525 [22-9915-2022](https://doi.org/10.5194/acp-22-9915-2022), 2022.

526 Xian, P., Zhang, J., O'Neill, N. T., Reid, J. S., Toth, T. D., Sorenson, B., Hyer, E. J., Campbell, J.  
527 R., and Ranjbar, K.: Arctic spring and summertime aerosol optical depth baseline from  
528 long-term observations and model reanalyses – Part 2: Statistics of extreme AOD events,  
529 and implications for the impact of regional biomass burning processes, *Atmos. Chem.*  
530 *Phys.*, 22, 9949–9967, <https://doi.org/10.5194/acp-22-9949-2022>, 2022.  
531